Influence of heat treatment on the fatigue resistance of Inconel 718 fabricated by selective laser melting (SLM)

Sasidharan Periane, Arnaud Duchon, Sébastien Vaudreuil, Hicham Chibane, Antoine Morandeau, René Leroy

Available online at www.sciencedirect.com

ScienceDirect

materialstoday: PROCEEDINGS

[ICMMM 2021]

Influence of heat treatment on the fatigue resistance of Inconel 718 fabricated by Selective Laser Melting (SLM)

S. Periane[a*], A. Duchosal[a], S.Vaudreuil[b], H.Chibane[c], A.Morandeau[d], M. Anthony Xavior[e], R. Leroy[a]

[a]*Univ. Tours, Univ. Orléans, INSA CVL, LaMé, 7 Avenue Marcel Dassault, Tours 37200, France,*
[b]*Euromed University of Fes (UEMF) – Fez,Morocco*
[c]*INSA Strasbourg, CSIP, ICube, 24 Boulevard de la Victoire,67084 Strasbourg Cedex, France*
[d]*Advanced Assisted Manufacturing Solutions (AAMS), Bâtiment CEROC, Rue Henri Garih, 37230 Fondettes, France*
[e]*Manufacturing Department, School of Mechanical Engineering, VIT University, Vellore - 632014, India*

* Corresponding author. Tel.: +33 (0) 761034269 ; *E-mail address:* sasinc87@gmail.com

Abstract

In this research work, the influence of heat treatment on the fatigue resistance of Inconel 718 (IN718) fabricated by selective laser melting (SLM) and cast and wrought (C&W) process route was investigated. The optical image of the as-built sample shows melt pool layers, within the melt pool layers both cellular and columnar dendritic structure are visible. The hardness value of the SLM sample under as-built condition is around 34% less compared to the reference (C&W) IN718. The as-built Inconel 718 samples were heat treated under Hot Isostatic Pressing (HIP) and Aeronautic Heat Treatment (AHT) conditions. During heat treatment the tensile residual stresses accumulated in the as-built sample was reduced close to zero. The hardness value has increased nearly equal to the hardness value of the reference sample which is due to the precipitation formation and reduced porosity during heat treatment. To evaluate the fatigue limit, the four point bending fatigue tests were carried out. Results showed fatigue limit of the C&W samples is high compared to the SLM samples due to the differences in their microstructure. Within the SLM samples, the HIP+AHT SLM has survived more fatigue cycles at high stress levels compared to the SLM HIP samples. This is due to the presence of more porosity which acted as the crack initiation site and presence of δ phase in the SLM HIP samples.

Keywords: Inconel 718; additive manufacturing; SLM; HIP; AHT; Four-point bending fatigue

1. Introduction

Inconel 718 alloy consisting of face centered cubic (FCC)-matrix [1] have remarkable mechanical properties. So, it is used in steam turbine, jet engines where it is subjected to high thermomechanical loads. It also possesses high strength-to-weight ratio, excellent resistance to fatigue, creep and corrosion. The above properties of Inconel 718 is due to the presences of special strengthening precipitates like γ'-Ni_3(Al, Ti) and γ"-Ni_3Nb [2]. By using the SLM technique parts can be fabricated with less material usage which is impossible with the conventional methods. The parts were fabricated in an inert, protective gas, like Nitrogen (Ni) or Argon (Ar) environment [3]. The laser power used is sufficient enough to melt the powder to a required depth in order to form a correct metallurgical bonding during solidification. The microstructure of the as-built IN718 samples cut parallel to the build direction shows the melt pool morphology and laser scanning paths perpendicular to the build direction [4]. The columnar dendrite growing epitaxially and surpassing many melt pool layers along the building direction were visible [5]. In addition, many defects like thermal cracks and porosity were observed. Y. Chen et al. studied that the grain boundary misorientation leads to liquation cracking (thermal cracks) which can be reduced by increasing the base cooling

effect during the deposition [6]. The porosity could have been inherited from the powder particles [7] or due to the entrapment of the gas particles during fabrication [8]. In addition to porosity another big challenge with the additive parts is the anisotropy which occurs due to the thermal variation during fabrication. The anisotropy and the porosity can be minimized by subjecting the as-built samples to heat treatments like HIP and AHT. The HIP is very essential for parts made of powder to improve its material properties and to reduce the porosity in order to maximize the working life of the parts [9]. During the HIP process the temperature is above 1000°C where the nucleation of the δ phase begins at the grain boundary into thin plates like structure which resists undesirable grain growth [10]. Normally γ'' precipitate is witnessed prior to the δ phase formation as the temperature raises from 600°C to above 1000°C. Since the chemical composition of both the phases have Nb content, as the temperature raises the δ phase forms at the expense of the γ'' precipitate. Even though δ phase is thermodynamically stable (resists notch brittleness) [11], its presence reduces hardenability and ductility due to the depletion of γ'' precipitate [12]. In order to improve the strength and ductility by means of the strengthening precipitates, a standard age hardening heat treatment like AHT is performed [4]. The purpose of AHT heat treatment is to dissolve the segregation of the particles and facilitate the population of the strengthening precipitates [13]. There were limited studies relating the influence of heat treatment (varied microstructure) to the fatigue properties. In this study the fatigue limit was determined by experimental method (iterative approach). To understand the influence of the heat treatment on the fatigue limit, a comparison is made between the fatigue limit of the SLM in both HIP and HIP+AHT condition with reference to the C&W samples.

2. Experimental methods

2.1. Sample fabrication

The gas-atomized (GA) spherical IN718 powder was used for fabrication of a nominal size ranging from 20 to 60 µm. The powder morphology has fine satellite particles attached to the main-sized powder particle but the powder had good flowability. The cast and wrought IN718 used in this study are commercial IN718 alloy. The nominal chemical composition of the powder in weight percentage are listed in Table 1.

Table 1. Nominal composition of the IN718 (wt.%).

Element	Al	Co	Cr	Cu	Ti	Mn	Mo	Nb+Ta	Ni	Fe
wt. %	0.2	1.0	21.0	0.3	1.15	0.35	3.30	5.50	55.0	Bal.

The samples were fabricated using the SLM 125 HL machine equipped with a maximum 400 W Yb-fiber laser in a build area (125 × 125 × 125 mm, L ×W× H). The laser power of 275 W with scanning speed ranging from 760 mm/s, hatch distance of 120 µm and the layer thickness of 50 µm with minimum scanning time of 12 seconds. The strips fill pattern type was used for the laser scan direction which was rotated 67° between the adjacent layers to reduce the residual stress as shown in Fig. 1(a). The fabrication was done on a pre heated built platform maintained at a temperature of 200°C in a controlled nitrogen atmosphere. The oxygen content was controlled less than 0.03% to avoid oxidation. The longitudinal samples were oriented parallel to the laser beam direction (X-Z plane). The fabricated longitudinal oriented SLM IN718 sample of length 60mm is shown in the Fig. 1 (b).

(a) (b)

Fig. 1. (a) Schematic representation of laser scanning strategy used in SLM experiments; (b) Longitudinal SLM IN718 samples.

2.2. Heat treatment

In order to obtain the density and the strength equal to that of the cast and wrought IN718, the SLM-IN718 specimens were subjected to different standard heat treatment which are listed in Table 2. The heat treatment effect on the microstructural and the mechanical properties of SLM-IN718 were also verified.

Table 2 : Designation of the heat treatment process for the SLM-IN718 specimens IN718, FC: furnace cooling; AC: air cooling; RC: rapid cooling.

Hot Isostatic Pressing (HIP)	1160°C/102 MPa/3h/RC
Aeronautic Heat Treatment (AHT)	720°C/8 h/FC→620°C/8 h/AC

The conventional (C&W) IN718 sample used for this study was age hardened and forged. In order to attain nearly the same density and the mechanical properties as conventional sample (C&W), one set of as-built samples were subjected to Hot isostatic pressing labelled as HIP. The HIP was carried out in inert argon gas atmosphere. Another set of samples were subjected to both HIP and Aeronautic heat treatment (AHT) denoted as HIP+AHT.

2.3. Specimen preparation and mechanical characterization

For the microstructural analysis, the specimen was cross sectioned along the building direction and then hot mounted using the Labopress -3 automatic mounting press. The mounted samples were then mechanically polished starting with 500 grit silicon-carbide paper down to 1200 grit and 3 to 1 µm diamond suspension slurries using Tegrapol -11 machine. To reveal the microstructural features, the polished specimens were then etched with the Kalling II reagent. An optical microscope Keyence VHX-2000 digital was used for the characterization. The higher magnification was performed under Scanning Electron Microscope (SEM). The mechanical characterization was performed using Vickers microhardness tester on polished specimens. The load was set to 20 kgf with a dwell time of 15s. The microhardness tests were performed in ambient conditions and 20-25 hardness indents were recorded on

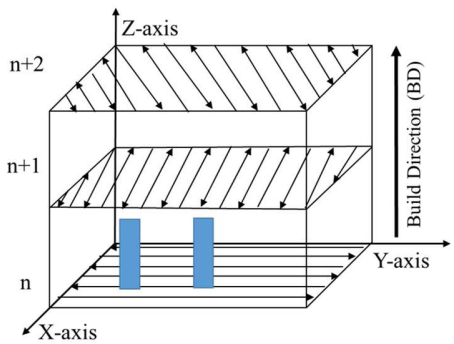

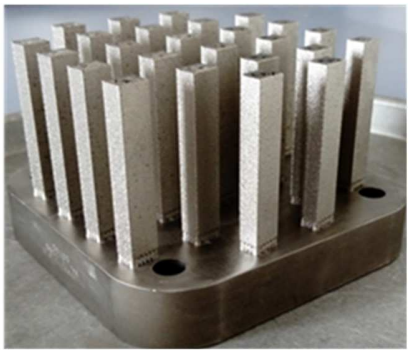

each analyzed cross-section. The surface roughness value (Ra, µm) is performed as per ISO 4287 standard the measured using 3D optical profilometer WYKO NT1100. The surface is measured using the 20X magnification. The

measured length of the sample was 4 mm. The residual stress measurement was determined using Bruker XRD device. The diffraction pattern was acquired using a MnKα X-ray radiation source, the {311} lattice plane spacings at a 2θ angle of about 153°. The residual stress was determined at six positions at a distance of 7 mm for as-built and heat-treated samples.

2.4. Fatigue tests

The four-point bending fatigue test, is a constant amplitude load-controlled test that was done using Instron 8872 equipped with servo hydraulic actuator. The machine is equipped with a ± 25kN patented Dyna load cell featuring compensation for inertial loads caused by heavy grips and fixtures. The samples are always placed in the same direction of machining. The test was conducted at a frequency of 20Hz and at a load ratio of 0.1 at room temperature. The four-point bending fatigue machine setup is shown in Fig. 2. The samples were placed in between the top loading rollers and the bottom support rollers, the distance maintained between the top loading rollers is 10 mm and for the bottom support rollers is 30 mm.

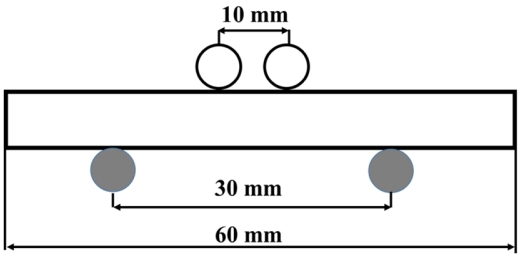

Fig. 2. The sketch of the four-point bending fatigue test set up of Instron 8872 machine.

3. Results and discussion

3.1. Microstructural analysis

The melt pool layers on the section parallel to the building direction was observed in Fig. 3 (a), the width and the length were hundreds of micrometers as a result of processing parameters. The width of the melt pool was approximately 118 µm were nearly equivalent to the chosen hatch distance of 120 µm. A small section of the melt pool boundary is enlarged in Fig. 3 (b) represents the elongated columnar microdentritic structures crossing the grain boundary. The columnar dendrite (region1) surpasses many melt-pool layers and oriented along the heat flux direction. The region 2 is the cellular dendritic structure which was formed due to the accumulation of the heat generated during the formation of the deep molten pools. The melted tracks are overlapped forming a strong metallurgical bonding between the adjacent layer. The transition from columnar to equiaxed is highlighted in the red region. Due to the rapid heating, melting and solidification of the alloy by the moving heat source the given energy input may not be sufficient to completely melt the powder particles which results in the presence of unmelt powder particles as seen in the Fig. 3 (c). The major defect witnessed in all the as-built parts are lack of fusion and porosity due to the entrapment of the gas generated during fabrication as in Fig. 3 (d).

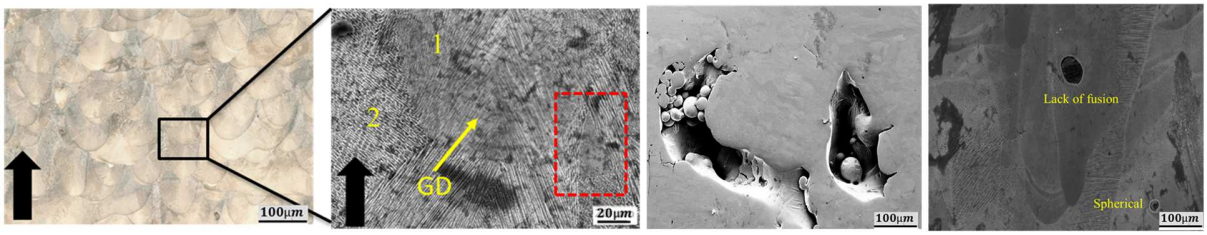

(a) (b) (c) (d)

Fig. 3. As-built IN718 microstructure with melt-pools (a) parallel to the building direction (the black arrow refers the build direction); (b) Columnar (1) and cellular dendrites (2), the black arrow refers the build direction and the yellow arrow refers to

the grain growth direction (GD) surpassing the melt pool layers, the red highlighted region is the grain growth and columnar and equiaxed transition region; (c) Un-melted powders; (d) porosity like lack of fusion and spherical pore.

The GA processed powder often contain entrapped gas bubbles. Despite fabricating with optimized parameters, the entrapped gas bubbles cannot necessarily escape from the melt due to rapid solidification process. Accumulation of these defects have a major negative influence on the mechanical properties.

3.2. Hardness

The hardness of the cast and wrought and the SLM IN718 (both in as-built and heat-treated conditions) were measured as represented in Fig. 4.

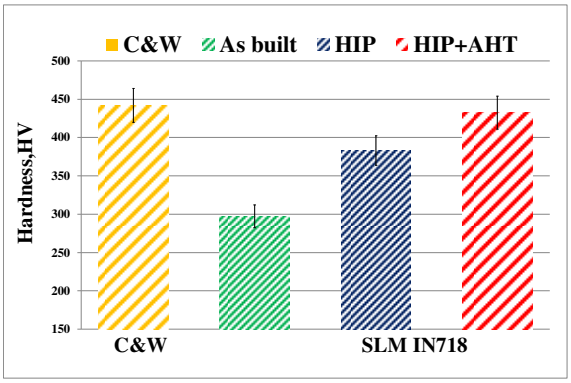

Fig. 4. Hardness value of reference (C&W), as-built, HIP and HIP+AHT SLM samples.

Comparing the as-built and heat-treated samples the precipitate formation and distribution during the heat treatment was verified with the hardness test. The hardness of the SLM sample after HIP+AHT is comparable to that of the hardness of C&W alloy. The increase in the hardness value of the SLM IN718 sample is due to the higher content of Nb available for γ'' precipitation. The Laves phase and δ phase present after HIP heat treatment predominantly consume the Nb available for the precipitation of γ'', which is the reason for HIP sample having low hardness compared to HIP+AHT sample. This shows the evidence that the heat treated SLM IN718 have material property comparable to C&W alloy.

3.3. Surface roughness

The surface roughness of the SLM IN718 sample under as-built condition was 19±4 µm. Since this surface roughness is not suitable for the fatigue test as roughness may be crack initiating sites. All the samples after heat treatment were machined using emulsion (USINOV 2475 from IGOL). The machining conditions were cutting speed (V_c) = 30 m/min, feed rate (f_z) = 0.1 mm/tooth, axial depth of cut (a_p) = 0.5 mm, radial depth of cut (a_e)= 9 mm and the length (L) of the sample = 60 mm at an emulsion pressure of 30 bar. After machining the average surface roughness of 0.32±0.05 µm was attained.

3.4. Residual stress

In general, parts fabricated using additive manufacturing technique experiences complex thermal histories (solidification shrinkage and thermal contraction of the solid). It results in the accumulation of tensile residual stresses of about 129±20 MPa. The tensile residual stress was developed by the liquid-state cracking mechanism formed during SLM process leads to thermal cracking. The tensile residual stress is completely relieved (26±5 MPa) after the heat treatment process (HIP+AHT) as the samples were maintained at a constant temperature for long time (annealing effect). The heat treatment process is very essential for additive samples not only to increase the properties and also to relieve the accumulated residual stresses during fabrication which is evident from the Fig. 5. On subjecting the samples to machining which induces compressive residual stress due to accumulation of thermo-mechanical stress during the machining process. After the machining process the samples have compressive residual

stress of (-)253±70 MPa. This induced compressive residual stresses by machining process are beneficial in sustaining the samples for more fatigue cycles before fatigue failure.

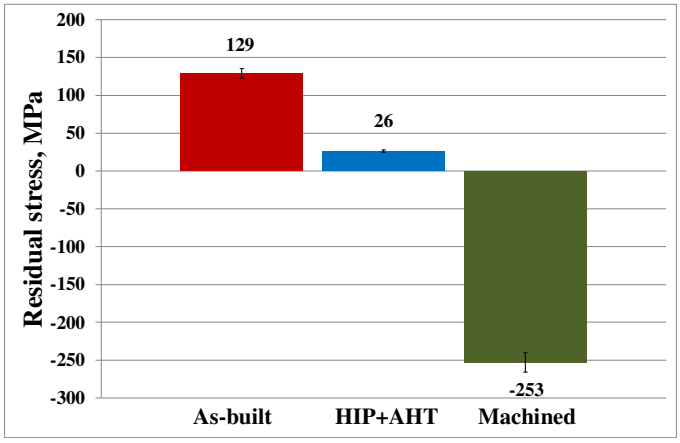

Fig. 5. Residual stress measurement values of the SLM IN718 in as-built, heat treated (HIP+AHT) and in machined condition.

3.5. Four-point bending fatigue tests

The fatigue strength of both SLM and C&W sample was determined using the staircase method with the samples of average surface roughness (Ra) 0.32±0.05 µm. The result from the fatigue testing of SLM heat-treated samples both HIP and HIP+AHT with reference to the C&W sample is presented in Fig. 6. As evident from the figure, there is a notable difference in the fatigue strength between the SLM and C&W specimens. The C&W sample has the highest fatigue limit with reference to SLM samples. It is evident from the overview of the fracture surface of the C&W sample shown in Fig. 7 (a) the crack propagation is until the final surface of the sample. In addition, the crack initiation is single and large (Fig. 7-b) unlike the SLM samples. Many high energy dimples were observed along the crack path represented in the Fig. 7 (c).

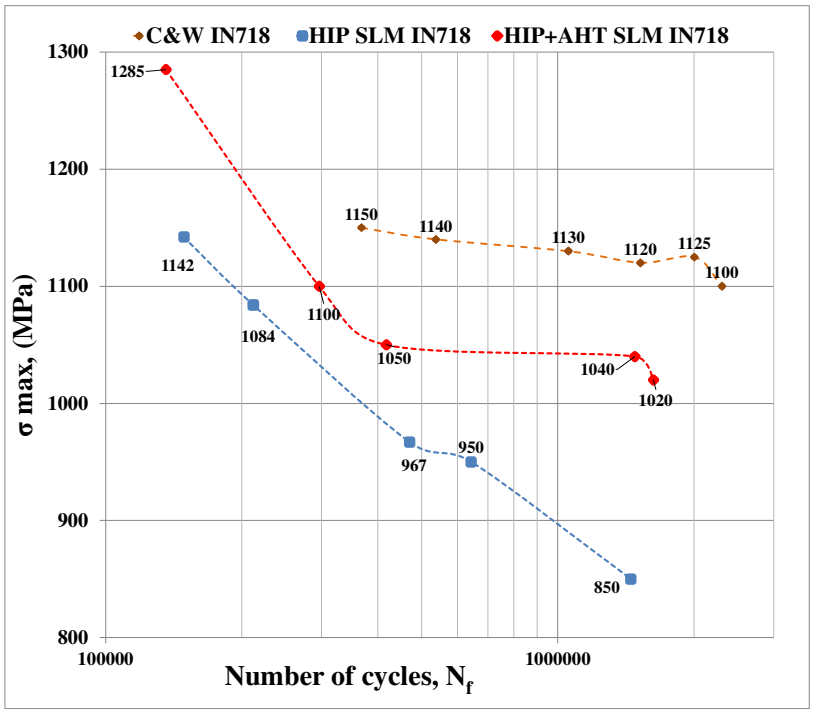

Fig. 6. σ-N curves for HIP and HIP+AHT samples in comparison to C&W IN718.

Comparing the fatigue strength of the HIP SLM with the HIP+AHT SLM samples. The HIP+AHT sample sustained for more fatigue cycles at high stress levels. It's quite obvious on comparing the transition area from the crack propagation to the final fracture from the overview of the fractured surface of the HIP SLM (Fig. 7-d) and the HIP+AHT SLM (Fig. 7-g). The reason for the least fatigue strength of the HIP SLM samples is due to the presence of porosity at the surface. The crack propagation initiates from the already existing pores highlighted on the surface shown in the Fig. 7 (e). Even after the HIP+AHT heat treatment presence of the pores on the surface were visible which is one among the reason for the multiple crack initiation. In general, the HIP+AHT samples have 20% more fatigue stress resistance and can withstand 6% more fatigue life cycles compared to the HIP samples due to the presence of the strengthening precipitates.

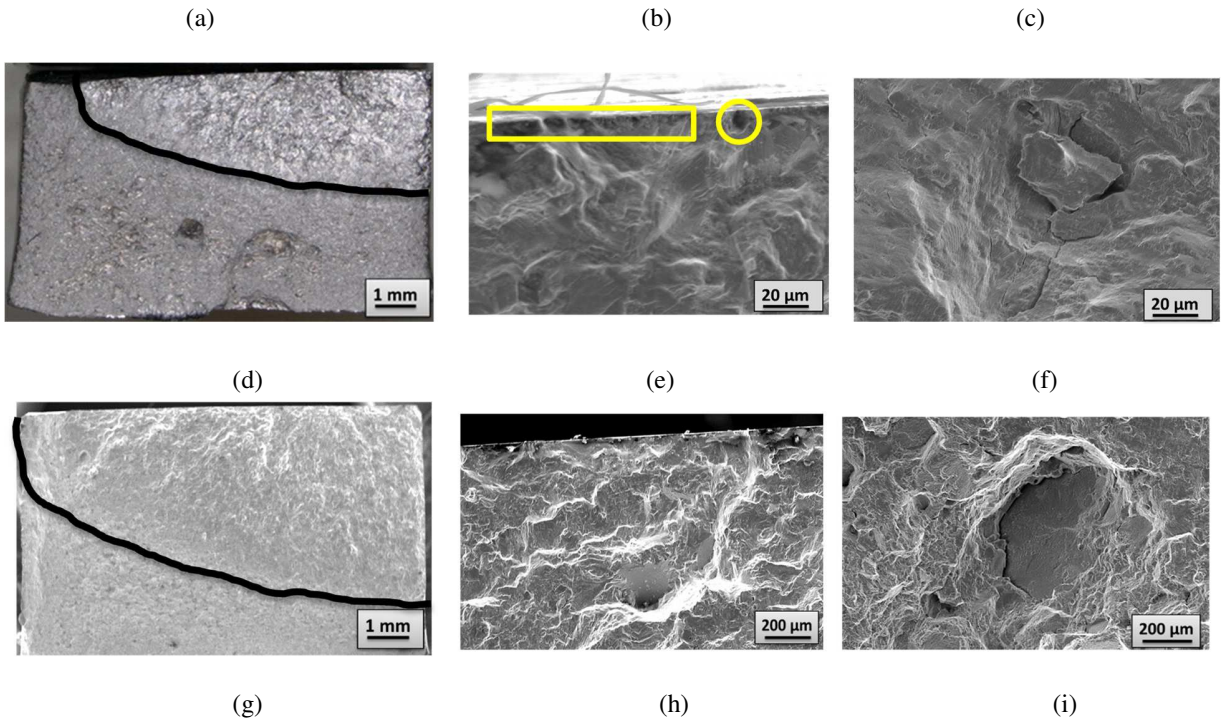

Fig. 7. The SEM image of fracture surfaces. (a) Overview of the fracture surface of a C&W IN718 specimen; (b) crack initiation with striations; (c) high energy dimples along the crack path; (d) Overview of the fracture surface of the HIP SLM IN718 specimen; (e) Crack propagation from the existing pores at the surface; (f) separated particle along the crack path; (g) Overview of the fracture surface of a HIP+AHT SLM IN718 specimen; (h) multiple crack initiation; and (i) Intergranular fracture.

4. Conclusions

The homogenized grain structure along with the presence of precipitates have enhanced the mechanical properties by increase in the hardness value up to 30% with reference to the as-built samples. The tensile residual stress has also reduced up to 87% due to the annealing process during AHT heat treatment. The machining improves fatigue

life by inducing compressive residual stress. The fractured surface of the HIP+AHT sample is more ductile. The difference in the fatigue life for HIP sample is due to the presence of the porosity at the surface which facilitated the crack propagation from the already existing pore. The surface pores were also the reason for the multiple crack initiation compared to C&W fractured surface with single large crack. The fractured surface of the C&W also shows the presence of high energy dimples along the crack path which is the reason for C&W samples sustained more fatigue cycles at high stress levels.

Acknowledgements

The authors would like to thank, Tool research center operators (CEROC, France) for machining support and Centre of study and research of elastomers materials engineer (CERMEL, France) for facilitating fatigue machine.

References

[1] B. Hassan, J. Corney, Grain boundary precipitation in Inconel 718 and ATI 718Plus, Mater. Sci. Technol. (United Kingdom). 33 (2017) 1879–1889. https://doi.org/10.1080/02670836.2017.1333222.

[2] A. Strondl, R. Fischer, G. Frommeyer, A. Schneider, Investigations of MX and γ′/γ″ precipitates in the nickel-based superalloy 718 produced by electron beam melting, Mater. Sci. Eng. A. 480 (2008) 138–147. https://doi.org/10.1016/j.msea.2007.07.012.

[3] M. Schmidt, M. Merklein, D. Bourell, D. Dimitrov, T. Hausotte, K. Wegener, L. Overmeyer, F. Vollertsen, G.N. Levy, Laser based additive manufacturing in industry and academia, CIRP Ann. 66 (2017) 561–583. https://doi.org/10.1016/j.cirp.2017.05.011.

[4] D. Zhang, W. Niu, X. Cao, Z. Liu, Effect of standard heat treatment on the microstructure and mechanical properties of selective laser melting manufactured Inconel 718 superalloy, Mater. Sci. Eng. A. 644 (2015) 32–40. https://doi.org/10.1016/j.msea.2015.06.021.

[5] Z. Wang, K. Guan, M. Gao, X. Li, X. Chen, X. Zeng, The microstructure and mechanical properties of deposited-IN718 by selective laser melting, J. Alloys Compd. 513 (2012) 518–523. https://doi.org/10.1016/j.jallcom.2011.10.107.

[6] Y. Chen, F. Lu, K. Zhang, P. Nie, S.R. Elmi Hosseini, K. Feng, Z. Li, Dendritic microstructure and hot cracking of laser additive manufactured Inconel 718 under improved base cooling, J. Alloys Compd. 670 (2016) 312–321. https://doi.org/10.1016/j.jallcom.2016.01.250.

[7] D. Deng, R.L. Peng, H. Brodin, J. Moverare, Microstructure and mechanical properties of Inconel 718 produced by selective laser melting: Sample orientation dependence and effects of post heat treatments, Mater. Sci. Eng. A. 713 (2018) 294–306. https://doi.org/10.1016/j.msea.2017.12.043.

[8] T.A. Faculty, A. Basak, I.P. Fulfillment, Advanced Powder Bed Fusion-Based Additive Manufacturing with Turbine Engine Hot-Section Alloys through Scanning Laser Epitaxy Advanced Powder Bed Fusion-Based Additive Manufacturing with Turbine Engine Hot-Section Alloys through Scanning Laser Epitaxy, (2017).

[9] M.E. Aydinöz, F. Brenne, M. Schaper, C. Schaak, W. Tillmann, J. Nellesen, T. Niendorf, On the microstructural and mechanical properties of post-treated additively manufactured Inconel 718 superalloy under quasi-static and cyclic loading, Mater. Sci. Eng. A. 669 (2016) 246–258. https://doi.org/10.1016/j.msea.2016.05.089.

[10] S. Azadian, L.Y. Wei, R. Warren, Delta phase precipitation in inconel 718, Mater. Charact. 53 (2004) 7–16. https://doi.org/10.1016/j.matchar.2004.07.004.

[11] D.F. Paulonis, J.J. Schirra, Alloy 718 at Pratt & Whitney–Historical Perspective and Future Challenges, Superalloys. 718 (2001) 13–23. https://doi.org/10.7449/2001/Superalloys_2001_13_23.

[12] P. Páramo-kañetas, M. Guerrero-mata, U. Özturk, J. Calvo, J.M. Cabrera, High-temperature deformation of delta-processed Inconel 718, J. Mater. Process. Tech. 255 (2018) 204–211. https://doi.org/10.1016/j.jmatprotec.2017.12.014.

[13] T. Alam, M. Chaturvedi, S.P. Ringer, J.M. Cairney, Precipitation and clustering in the early stages of ageing in Inconel 718, Mater. Sci. Eng. A. (2010). https://doi.org/10.1016/j.msea.2010.08.053.

[14] A. Cellier, F. Chalon, V. Grimal-Perrigouas, D. Bonhoure, R. Leroy, Effects of cutting angles in Ti-6al-4v Milling process on surface integrity: Influence of roughness and residual stresses on fatigue limit, Mach. Sci. Technol. 18 (2014) 565–584. https://doi.org/10.1080/10910344.2014.955369.